Influence of residual stress on thermal expansion behavior

X.-L. Wang,[a] C. M. Hoffmann, C. H. Hsueh, G. Sarma, C. R. Hubbard, and J. R. Keiser
Oak Ridge National Laboratory, Oak Ridge, Tennessee 37831-6064

(Received 17 August 1999; accepted for publication 20 September 1999)

We demonstrate that the thermal expansion behavior of a material can be substantially modified by the presence of residual stresses. In the case of a composite tube made of two layers of dissimilar steels, *in situ* neutron diffraction measurements revealed a significant difference in the coefficients of thermal expansion along the radial and tangential directions. It is shown that the observed difference in thermal expansion is due to the change of residual stresses with temperature. © *1999 American Institute of Physics.* [S0003-6951(99)01647-2]

Thermal expansion is a fundamental property of a material, arising from the anharmonic vibration of the crystal lattice. For a single crystal under no external influence, its coefficient of thermal expansion (CTE) is compliant with the crystal symmetry.[1] For instance, the CTE of a cubic crystal is isotropic along different crystallographic directions. While the thermal expansion behaviors of simple materials are relatively well understood, there have been continuing studies of the thermal expansion behaviors of complex materials systems, such as ceramic–ceramic and ceramic–metal composites.[2–4] Depending on the microstructure, the overall thermal expansion of a composite material may differ from that given by constitutive models.[2]

In practical applications, thermal expansion is an important consideration, not only from the thermophysical property point of view but also from the standpoint of the mechanical behavior of the material. This is because in a fabricated component, differences in thermal expansion between constituent materials lead to thermal residual stresses, which affect the integrity and lifetime of the component.

The design of replacement materials for composite tubing used in Kraft black liquor recovery boilers[5,6] is a case in point. A composite tube is made of a carbon steel core and a corrosion-resistant clad layer. Because of the thermal expansion mismatch between the carbon steel and clad layers, thermal residual stresses are generated as the boiler goes through operating cycles. Experimental and finite-element studies have shown that the signs and magnitudes of these residual stresses are dictated by the difference in CTE (between the two layers of dissimilar materials) and the yield strength of the clad layer.[6] If the clad layer is in tension, as is the case for composite tubing currently in use, the boiler is vulnerable to stress-corrosion cracking, which could lead to grave economical consequences and causes safety concerns as well.

Accurate modeling of thermal residual stresses depends on detailed knowledge of the thermal expansion behaviors of the constituent materials. We show here that under the influence of residual stresses, the thermal expansion behavior of a material may be substantially different from that in the unconstrained condition. As will be shown below, for samples containing type-I or macroresidual stresses, the effective coefficient of thermal expansion as measured in a diffraction experiment may be *macroscopically* anisotropic.

The specimen is a 2.5-in.-o.d. composite tube. The core part of the tubing is SA 210 carbon steel, with the composition 0.18C–0.28Si–0.65Mn–0.006P–0.15S wt %.[7] The clad layer is Sanicro 28, a nickel-based austenitic alloy steel, with the composition 0.10C–26.7Cr–30.4Ni–3.33Mo–36.2Fe–0.01Nb–1.06Cu wt %.[8] A cross-sectional view of the specimen is shown in Fig. 1. The geometric dimensions are $a=24.8\,\text{mm}$, $b=30.0\,\text{mm}$, $c=31.8\,\text{mm}$, and $l=300\,\text{mm}$. Table I lists the coefficients of thermal expansion and elastic properties[7,8] for each material comprising the tube specimen.

The neutron diffraction experiment was conducted at the High Flux Isotope Reactor of Oak Ridge National Laboratory, using the HB-2 spectrometer modified for residual stress mapping.[9] The specimen was mounted upright and slits of $1\times30\,\text{mm}^2$ and $1\times50\,\text{mm}^2$ were inserted before and after the specimen, which together defined a sampling volume of approximately 30 mm.[3] A heating tape wrapped around the tube specimen provided controlled heating up to 250 °C. Temperatures within the tube were monitored with eight thermocouples, four on the inside and four on the outside surfaces, respectively. A rather uniform temperature field was achieved with the present experimental setup; the maximum difference in temperatures recorded by the thermocouples was less than 2 °C. Detailed strain measurements were made in the middle of the carbon steel, using the bcc (2 1 1) peak. At each location, diffraction peaks were recorded for two specimen orientations, with the scattering vector par-

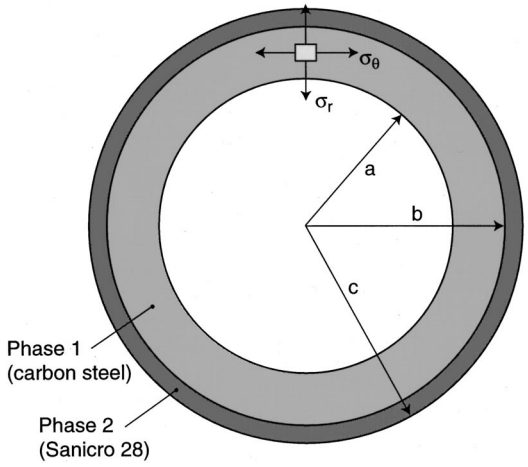

FIG. 1. Schematic of a cross-sectional view of the tube specimen used in neutron diffraction measurements.

[a]Electronic mail: wangxl@ornl.gov

TABLE I. Coefficients of thermal expansion (α), Young's modulus (E), and Poisson's ratio (ν) for the carbon steel core[a] and Sanicro 28 clad layer.[b]

	α(30–250 °C) (10^{-6} °C^{-1})	E(30 °C) (GPa)	ν(30 °C)
Carbon steel core	13.3	207	0.29
Sanicro 28 clad layer	16.0	195	0.29

[a]Reference 7.
[b]Reference 8.

allel to the radial and tangential directions, respectively. The fitted peak position was then used to calculate the effective thermal expansion for each orientation, using the following equation:

$$\epsilon = \frac{d(T) - d(T_0)}{d(T_0)} = \frac{\sin\theta(T_0)}{\sin\theta(T)} - 1, \tag{1}$$

where d is the lattice spacing corresponding to the measured peak, 2θ is the diffraction angle, and T_0 is room temperature ($\sim$30 °C).

Figure 2 shows the experimentally determined thermal expansion for two specimen orientations, with the scattering vector parallel to radial and tangential directions, respectively. As can be seen, the effective thermal expansion varies linearly with temperature. No hysteresis was observed for cycling between room temperature and 250 °C, indicating that the thermally induced deformation is fully elastic within the temperature range of study (see Ref. 6 and also below). At a given temperature, the effective thermal expansion in the tangential direction ϵ_θ is always greater than that in the radial direction ϵ_r. This shows that the effective thermal expansion, as determined in the present neutron diffraction experiment, is macroscopically anisotropic. The effective CTE were determined by fitting the data to straight lines, and the results are $\alpha_\theta^* = 13.7\times10^{-6}\,\mathrm{C}^{-1}$ and $\alpha_r^* = 12.8\times10^{-6}\,\mathrm{C}^{-1}$. These values can be compared with the published CTE for carbon steel, which is $13.3\times10^{-6}\,\mathrm{C}^{-1}$.[7]

The difference in α_θ^* and α_r^* can be qualitatively understood by considering that the measured lattice spacing contains a temperature-dependent elastic component, i.e.,

$$d(T) = d_0(T)(1+\epsilon(T)), \tag{2}$$

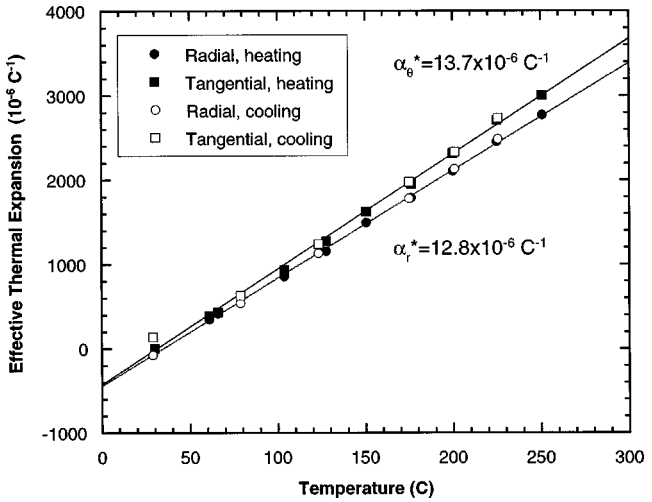

FIG. 2. Effective thermal expansion in carbon steel as a function of temperature. The solid lines are linear fits to the experimental data.

where d_0 denotes the lattice spacing under the unconstrained (stress-free) condition and $\epsilon(T)$ the residual strain at a given temperature. To facilitate the discussions, we rewrite $\epsilon(T)$ as

$$\epsilon(T) = \epsilon_0 + \epsilon'(T), \tag{3}$$

where ϵ_0 is the residual strain at room temperature, and $\epsilon'(T)$ is the thermally induced elastic strain such that $\epsilon' = 0$, when $T = T_0$. By differentiating Eq. (2), the effective CTE is obtained,

$$\alpha^* = \frac{1}{d}\frac{\partial d(T)}{\partial T} = \alpha + \frac{\partial \epsilon'}{\partial T}, \tag{4}$$

where $\alpha = (1/d_0)\partial d_0(T)/\partial T$ is the CTE under the unconstrained condition. Equation (4) shows that the effective CTE as measured in a diffraction experiment is modified by the thermal stress induced during heating. Moreover, the effective CTE is *macroscopically* anisotropic (i.e., dependent on specimen directions), unless the thermally induced residual stress is hydrostatic. For the composite tubing used in this study, $\epsilon'_\theta(T)$ in the carbon steel layer is tensile upon heating, due to the larger CTE of the clad layer, and increases with temperature. As a consequence, $\alpha_\theta^* > \alpha$. Because of the small wall thickness, the radial stress is small throughout the tube[10] and, therefore, the elastic strain in the radial direction is mostly due to the Poisson's effect. This leads to the observed $\alpha_r^* < \alpha$.

To further understand the difference between α_θ^* and α_r^*, we have carried out an analytical calculation of the thermal residual stresses in composite tubes due to thermal expansion mismatch. The analytical model is illustrated in Fig. 1, in which a cylindrical shell of phase 1 with an inner radius a and an outer radius b is surrounded by a concentric cylindrical shell of phase 2 with an outer radius c. Stresses are analyzed for locations away from the ends of the cylindrical shells and the free-end effects are not considered. The stresses can be determined by the procedure of first allowing the two phases to exhibit unconstrained thermal strains during the temperature change ΔT. Then, the radial traction σ_b is placed at the interfaces $r = b$, and axial tractions $\sigma_{1,z}$ and $\sigma_{2,z}$ are placed on phases 1 and 2, respectively, to restore the displacement continuity between the two phases. The axial tractions are subjected to the requirement that the resultant axial force be zero since no external force is applied on the system. Details of the analysis are reported elsewhere,[11] but the solution for stresses in phase 1 is given below:

$$\sigma_{1,r} = \frac{b^2(r^2-a^2)}{r^2(b^2-a^2)}\sigma_b, \tag{5a}$$

$$\sigma_{1,\theta} = \frac{b^2(r^2+a^2)}{r^2(b^2-a^2)}\sigma_b, \tag{5b}$$

$$\sigma_{1,z} = \frac{P_1 - P_3}{P_4 - P_2}\sigma_b, \tag{5c}$$

where σ_b is given by

$$\sigma_b = \frac{(P_4 - P_2)E_1(\alpha_2 - \alpha_1)\Delta T}{P_1P_4 - P_2P_3}. \tag{6}$$

In Eq. (6), $\Delta T = T - T_0$, and E and α are the Young's modulus and unconstrained CTE. The subscripts in E and α denote

phases 1 and 2, respectively. P_1, P_2, P_3, and P_4, are constants related to a, b, c, and E, ν, α of both phases, where ν is the Poisson's ratio of the material. Following Hooke's law, the elastic strains in phase 1 were obtained,

$$\epsilon'_{1,j}=\frac{(1+\nu_1)\sigma_{1,j}-\nu_1(\sigma_{1,r}+\sigma_{1,\theta}+\sigma_{1,z})}{E_1}, \tag{7}$$

where $j=r$, θ, and z.

From Eqs. (5)–(7), it can be seen that the thermally induced elastic strains are proportional to σ_b, which varies linearly with T. This explains why the effective thermal expansion shown in Fig. 2 remains linear with temperature. Substituting Eq. (7) into Eq. (4) and using the parameters in Table I, the contribution by thermal stress towards the effective CTE was determined. For middepth in the carbon steel, where the neutron diffraction measurements were made, these contributions are -0.5×10^{-6} C^{-1}, 0.6×10^{-6} C^{-1}, and 0.7×10^{-6} C^{-1}, respectively, along radial, tangential, and axial directions. Adding to the published value for α_1 (see Table I), we obtain the effective CTE in the carbon steel: $\alpha'_{1,r}=12.8\times10^{-6}$ C^{-1}, $\alpha'_{1,\theta}=13.9\times10^{-6}$ C^{-1}, and $\alpha'_{1,z}=14.0\times10^{-6}$ C^{-1}. The calculated values of $\alpha^*_{1,r}$ and $\alpha^*_{1,\theta}$ are in excellent agreement with the experimental data. With a similar analysis, it can be shown that the effective CTE in the clad layer is also anisotropic, but with an inverse anisotropy in the sense that $\alpha^*_{2,z}\simeq\alpha^*_{2,\theta}<\alpha^*_{2,r}$. This prediction was confirmed by subsequent neutron diffraction measurements in the clad layer of a similarly prepared composite tube.[11]

The example discussed in this letter illustrates the influence of residual stress on the thermal expansion behavior of a material. This phenomenon is ubiquitous in all materials whose residual stresses vary with temperature. It is generally accepted that residual stresses can be classified into three categories, depending on their length scale relative to the microstructure. Macro-, or type-I, stresses are uniform across several grains. Micro-, or type-II, stresses are uniform within a grain, but vary from grain to grain. Type-III stresses are referred to those that fluctuate within a grain. The example of composite tubing is specific to macrostresses, whose signs and magnitudes usually vary with specimen directions. Thus, in general, the effective CTE in specimens containing macroresidual stresses is expected to be macroscopically anisotropic. Note that this anisotropy is characteristically different from the intrinsic anisotropy along various crystallographic directions. The latter is a fundamental property of a material and is governed by the symmetry of the crystal lattice. The macroscopic anisotropy discussed here is due to external influence and, therefore, has no crystal symmetry requirement.

Microresidual stresses also affect the thermal expansion behavior. The effect of microresidual stresses is perhaps more readily realized in a two-phase composite material, where microresidual stresses are generated due to the thermal expansion mismatch between the two phases. Analysis of the residual stress and thermal expansion data obtained for Al_2O_3–ZrO_2 ceramic composites[12] indicates that the effective CTE in each phase is modified towards a reduced mismatch in CTE between the two phases. In addition, because residual stresses in a composite material depend in part on the microstructure, the overall thermal expansion of the composite may also differ from that given by constitutive models, as illustrated by Hsueh, Becher, and Sun.[2]

The interaction of residual stress and thermal expansion in a material has significant implications in practical applications. From a materials design point of view, the reliability of finite-element models that simulate the thermal–mechanical behavior of a material depends on the accuracy of the CTE used in the models. As noted earlier, the experimentally determined CTE may be substantially different from that in the unconstrained condition. A small deviation in the CTE of one phase could lead to a large error in the calculation of the CTE mismatch, which usually determines the thermal stress in the materials system. The complexity resulting from interaction between residual stress and thermal expansion also brings about, potentially, a new method in residual stress determination. As can be seen from Eqs. (3) and (7), by comparing the experimentally determined CTE for various specimen orientations with that in the unconstrained condition, it should be possible to derive information about the residual stresses in the material. This method can become particularly useful when a stress-free specimen required in conventional neutron diffraction measurements cannot be made. Of course, to apply this method, the unconstrained CTE must be known in advance.

In summary, the influence of residual stress on thermal expansion behavior was demonstrated with a composite tube made of two layers of dissimilar steels. The presence of a temperature-dependent residual stress causes the effective coefficients of thermal expansion to be significantly different along different specimen directions. Particular care must be taken when interpreting the experimental results from thermal expansion measurements.

This work was sponsored by the Advanced Industrial Materials Program, U.S. Department of Energy. Oak Ridge National Laboratory is managed by Lockheed Martin Energy Research Corporation for the U.S. Department of Energy under Contract No. DE-AC05-96OR22464.

[1] J. F. Nye, *Physical Properties of Crystals* (Oxford University Press, London, U.K., 1985), pp. 93–109.
[2] C. H. Hsueh, P. F. Becher, and E. Y. Sun (unpublished).
[3] Y.-L. Shen, Mater. Sci. Eng., A **252**, 269 (1998).
[4] M. Hoffman, S. Skirl, W. Pompe, and J. Rodel, Acta Mater. **47**, 565 (1999).
[5] J. R. Keiser, B. Taljat, X.-L. Wang, R. W. Swindeman, P. J. Masiasz, L. E. Meyers, R. L. Thomas, S. T. Elliot, D. L. Singbeil, and R. Prescott, in *Proceedings of the 9th International Symposium on Corrosion in the Pulp and Paper Industry* (Pulp and Paper Research Institute of Canada, Vancouver, Canada, 1998), pp. 213–220.
[6] B. Taljat, T. Zacharia, X.-L. Wang, J. R. Keiser, and R. W. Swindeman, in *Proceedings of the 9th International Symposium on Corrosion in the Pulp and Paper Industry* (Pulp and Paper Research Institute of Canada, Vancouver, Canada, 1998), pp. 193–197.
[7] *Materials Handbook, Desk Edition* (ASM International, Metals Park, OH, 1992).
[8] Data sheet for Sandvik Sanicro 28 austenitic stainless alloy, S-1885-ENG (March 1997 edition), Sandvik Steel AB, Sweden.
[9] X.-L. Wang, C. R. Hubbard, S. Spooner, S. A. David, B. H. Rabin, and R. L. Williamson, Mater. Sci. Eng., A **211**, 45 (1996).
[10] X.-L. Wang, E. A. Payzant, B. Taljat, C. R. Hubbard, J. R. Keiser, and M. J. Jirinec, Mater. Sci. Eng., A **232**, 31 (1997).
[11] X.-L. Wang (unpublished).
[12] K. B. Alexander, P. F. Becher, X.-L. Wang, and C. H. Hsueh, J. Am. Ceram. Soc. **78**, 291 (1995).